Technologies and Materials for Renewable Energy, Environment & Sustainability

Influence of Indium Substitution on the Morphological Properties of Hg-Based Thin Films Deposited by PLD

AIPCP25-CF-TMREES2025-00100 | Article

Influence of Indium Substitution on the Morphological Properties of Hg-Based Thin Films Deposited by PLD

Doaa Jameel Lafta[1, a)] and Haider MJ. Haider[1, b]

[1] *Kufa University - Faculty of Education for Girls- Physics Department, Najaf- Iraq*

[a)] *Doaaj.ail@student.uokufa.edu.iq*
[b)] *Corresponding author: hayderm.alhayderi@uokufa.edu.iq*

Abstract. Thin films of $Hg_{1-x}In_xBa_2Ca_2Cu_{2.8}Ti_{0.2}O_8$ were successfully synthesized using the pulsed laser deposition (PLD) technique with varying indium concentration ($0.0 \leq x \leq 0.2$). The effect of indium incorporation on the structural and morphological features of the films was systematically investigated. X-ray diffraction (XRD) patterns revealed a continuous enhancement in crystallinity with increasing In content, achieving an optimum order at x = 0.12, where the diffraction peaks became sharper and more intense, accompanied by a slight shift toward higher 2θ values, indicating c-axis contraction and improved lattice coherence. Field emission scanning electron microscopy (FESEM) and atomic force microscopy (AFM) analyses confirmed the structural observations, revealing a dense, homogeneous, and fine-grained nanostructure with minimal roughness at the same concentration. However, further increase in indium content ($x \geq 0.16$) resulted in microstructural degradation and the appearance of grain clustering due to excess strain and partial phase segregation. Overall, the study demonstrates that moderate indium substitution (x = 0.12) yields the most stable and compact nanostructure, representing the optimum condition for producing high-quality Hg-based superconducting thin films.

Keywords: Hg-based superconductors; Pulsed Laser Deposition (PLD); Indium substitution; XRD; FESEM; AFM; Morphology; Crystallinity; Thin films.

INTRODUCTION

High-temperature superconductors (HTS) are among the most remarkable materials in solid-state physics due to their unique properties, such as zero electrical resistance and perfect magnetic flux exclusion, which make them highly promising for applications in advanced electronics, magnetic levitation, and energy transport systems [1,2]. Among these systems, the mercury-based cuprates (Hg-based cuprates) occupy a special position because they exhibit the highest superconducting transition temperature (Tc ≈ 135 K) reported for the compound $HgBa_2Ca_2Cu_3O_{8+\delta}$(Hg-1223)[3]. Recent studies have shown that chemical substitution within these materials is an effective route to tune the crystal lattice and improve the morphological growth quality of thin films [4,5]. Indium (In^3) is one of the most promising elements to partially replace mercury (Hg^2) because of their similar ionization energies and its ability to enhance structural stability by reducing the ionic vacancies within the Hg–O layer, leading to improved lattice ordering and lower defect density [6]. Pulsed laser deposition (PLD) technique enables the fabrication of high-quality superconducting thin films with precise thickness control and fine nanostructural organization. Through careful adjustment of pulse energy and deposition rate, PLD can promote oriented or semi-epitaxial growth, which is essential for achieving strong crystallographic texture [7,8]. However, challenges in controlling the growth parameters—especially in systems containing volatile elements such as mercury—often lead to the formation of micrometer-sized droplets or secondary phases that affect surface smoothness and grain compactness [9]. Electron microscopy (FESEM) provide valuable insight into grain distribution, surface uniformity, and nanoscale roughness, which are directly related to crystal growth mechanisms and phase stability [10]. Complementary X-ray diffraction (XRD) analysis allows tracking of variations in crystal size and orientation as a function of indium substitution [11]. Based on this framework, the present work aims to investigate the morphological evolution resulting from partial indium substitution at the mercury site in the $Hg_{1-x}In_xBa_2Ca_2Cu_{2.8}Ti_{0.2}O_{8+\delta}$ system. A comprehensive analysis of AFM, FESEM, and XRD results across multiple indium concentrations ($0.0 \leq x \leq 0.2$) was performed to understand how nanostructural

organization and surface quality evolve with composition and to identify the optimum substitution level for homogeneous film growth.

EXPERIMENTAL

A series of superconducting thin films with the nominal composition $Hg_{1-x}In_xBa_2Ca_2Cu_{2.8}Ti_{0.2}O_{8+\delta}$ were prepared, where the indium substitution ratios at the mercury site were varied as x = 0.00, 0.04, 0.08, 0.12, 0.16, and 0.20. High-purity precursors (≥ 99.9%) of HgO, In_2O_3, $BaCO_3$ (or BaO), $CaCO_3$, CuO, and TiO_2 were accurately weighed according to the stoichiometric proportions of the target composition.

The PLD targets were fabricated using the conventional solid-state reaction (SSR) method. The powders were initially mixed in an agate mortar for about 30 min, then homogenized further using a mechanical mixer with steel balls for approximately one hour to ensure uniform blending. The resulting mixture was pressed into pellets of (1–2) cm diameter and (3–5) mm thickness under a high uniaxial pressure of about 9–10 tons. Preliminary sintering was carried out in an oxidizing atmosphere (air or O_2) at 750 °C for 24 h, followed by controlled cooling. To minimize mercury loss, the pellets were placed inside closed alumina crucibles during sintering.

Glass substrates were used for the deposition process. The substrates were sequentially cleaned in acetone, isopropanol, and deionized water using an ultrasonic bath for (10–15) minutes in each solvent, dried under pure nitrogen flow, and optionally treated with oxygen plasma to enhance surface energy and adhesion. Since glass is an amorphous material, the resulting films are expected to exhibit strong texture (highly oriented or randomly aligned) rather than perfect epitaxial growth as observed on crystalline substrates like MgO or SrTiO.Thin-film deposition was performed using a Nd: YAG laser operating at a wavelength of 1064 nm, with a pulse duration of (5–10) ns and a repetition rate of (5–10) Hz. The laser fluence on the target was maintained between (1.5 and 3.0) J/cm² at an incident angle of ≈ 45°, with a target–substrate distance of (4–5) cm. The deposition chamber was evacuated to (10^{-4}–10^{-5}) Torr, then backfilled with oxygen to the desired working pressure.After deposition, the films were subjected to post-annealing in flowing oxygen at (350–500) °C for (1–2) hours to improve oxygen ordering and structural stability. To further stabilize the superconducting phase and reduce mercury volatilization, the samples were cooled slowly in a controlled oxygen atmosphere.Through this procedure, dense and uniform nanostructured thin films were obtained, suitable for detailed structural and morphological characterization using XRD, FESEM, and AFM, as illustrated in Fig. 1.

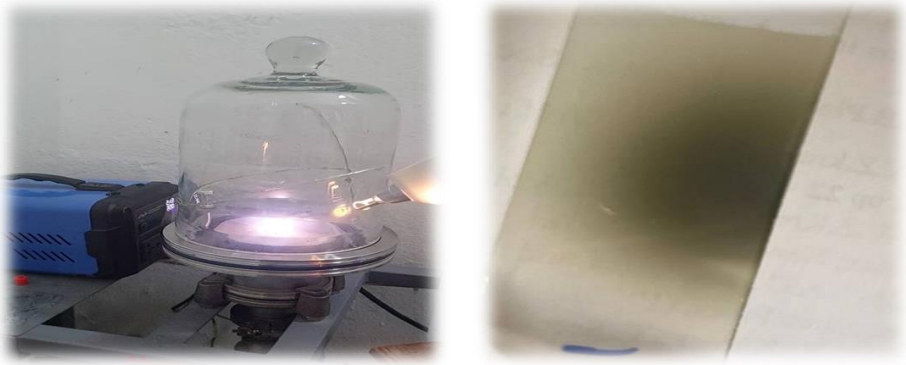

FIGURE 1. Photographic illustration of the prepared samples along with the pulsed laser deposition (PLD) system

RESULTS AND DISCUSSIONS

After the thin films were successfully prepared, the samples underwent a series of precise structural and morphological characterizations to investigate their crystalline structure and surface topography, aiming to understand the influence of indium substitution ratios on crystal growth and surface uniformity. X-ray diffraction (XRD) analysis was carried out using a Cu Kα radiation source (λ = 1.5406 Å) to identify the formed crystalline phases and to study the structural characteristics of the deposited films. The diffraction patterns were recorded within the angular range of 2θ = 10°–80° at a slow scan rate to enhance peak resolution. The obtained data were used to calculate the lattice parameters (a, b, c) and the c/a ratio, as well as to determine the average crystallite size (D) according to the Scherrer equation $D = \frac{K\lambda}{\beta \cos\theta}$, where K is the shape factor (≈0.9), λ is the X-ray wavelength, β is the full width at half maximum (FWHM) of the diffraction peak, and θ is the Bragg angle. The Miller indices (hkl) of the main reflections were identified by comparison with the standard JCPDS reference cards corresponding to mercury-based superconducting phases of the Hg-1212 type [12].To complement the structural findings, the surface morphology and grain structure of the thin films were examined using field-emission scanning electron microscopy (FESEM). Micrographs captured at various magnifications (ranging from 4,000× to 120,000×) revealed the evolution of the grain distribution, surface density, and overall homogeneity with increasing indium substitution. The analysis provided clear evidence of the relationship between surface texture and crystal growth behavior, showing variations in grain connectivity and compactness that reflect the influence of indium content on the film formation process [12].

TABLE 1. Shows the phase ratios, lattice parameters, and (c/a) ratio

X	a (A)	b (A)	C (A)	c/a	V $(A)^3$	Dm (gm/cm^3)
0	3.827954	3.827954	16.36864	4.27608	239.8535	6.049574
0.04	3.752286	3.752286	14.53819	3.87449	204.6926	7.063505
0.08	3.723132	3.723132	16.64873	4.4717	230.7799	6.242672
0.12	3.827954	3.827954	16.36864	4.27608	239.8535	5.984984
0.16	3.225517	3.225517	16.19028	5.019437	168.443	8.491626
0.20	3.84221	3.84221	16.0287	4.1717	236.6249	6.022996

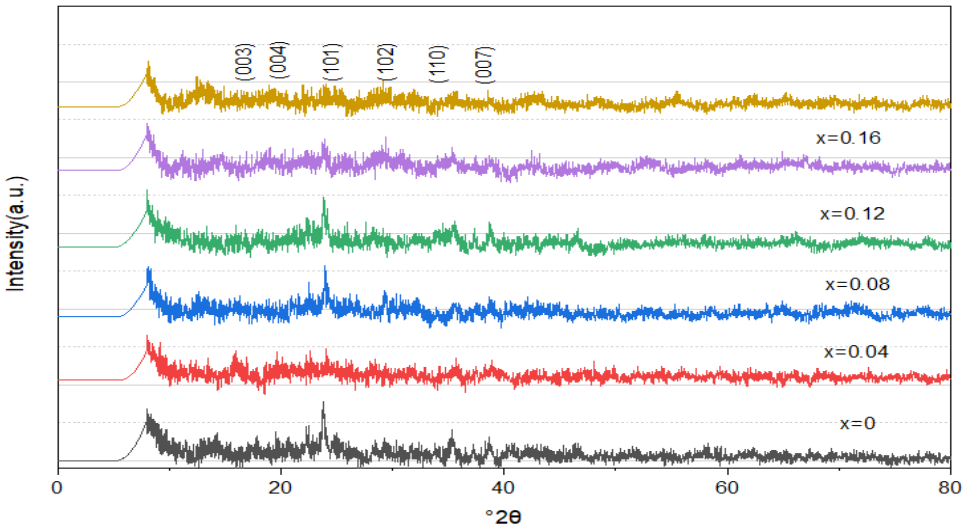

FIGURE 2. X-ray diffraction (XRD) patterns of $Hg_{1-x}In_xBa_2Ca_2Cu_{2.8}Ti_{0.2}O_{8+\delta}$ thin films prepared by PLD at different indium substitution levels (x = 0.00–0.16), showing the main diffraction peaks corresponding to the tetragonal phase and the evolution of peak intensity and position with increasing in content.

In addition, atomic force microscopy (AFM) was employed to characterize the nanoscale topography and quantify the surface roughness parameters. Three-dimensional AFM images were obtained over scan areas of (1×1) μm² and (5×5) μm², allowing precise measurement of the root mean square roughness (Sq), skewness (Ssk), kurtosis (Sku), and surface area ratio (SA/PA). The AFM analysis confirmed the improvement in surface smoothness and uniformity at intermediate substitution levels, corresponding to enhanced crystal ordering and reduced defect density observed in the XRD and FESEM results. The combined findings from these three techniques provided a comprehensive understanding of how indium substitution influences both the structural integrity and morphological quality of the $Hg_{1-x}In_xBa_2Ca_2Cu_{2.8}Ti_{0.2}O_{8+\delta}$ thin films.

The results obtained from X-ray diffraction (XRD), field-emission scanning electron microscopy (FESEM), and atomic force microscopy (AFM) revealed a clear evolution in both structural and morphological properties of the $Hg_{1-x}In_xBa_2Ca_2Cu_{2.8}Ti_{0.2}O_{8+\delta}$ thin films as the indium substitution ratio increased within the range ($0.0 \leq x \leq 0.2$). The XRD patterns showed that the reference film (x = 0.00) exhibited broad and weak diffraction peaks, indicating limited crystallinity and the possible presence of secondary phases or structural imperfections caused by partial mercury volatilization during deposition [13].

At low substitution levels (x = 0.04–0.08), the diffraction peaks became sharper and more intense with a noticeable reduction in full width at half maximum (FWHM), signifying an increase in crystallite size and a decrease in internal lattice strain. The main reflections (003), (004), (101), (102), (110), and (007) displayed a slight shift toward higher 2θ values ($\Delta 2\theta \approx +0.2°$ to $+0.4°$) compared to the undoped sample. This behavior is attributed to the substitution of smaller In^{3+} ions for the larger Hg^{2+} ions, resulting in a slight contraction along the c-axis and enhanced bonding within the Cu–O layers. At the intermediate composition (x = 0.12), the diffraction peaks reached them [14].

maximum sharpness and intensity, accompanied by strong c-axis-oriented growth, which reflects the highest degree of crystallinity and structural stability. However, at higher substitution levels ($x \geq 0.16$), the peaks became broader and less intense, shifting slightly toward lower angles ($\Delta 2\theta \approx -0.2°$ to $-0.3°$), indicating an expansion of the c-axis, increased lattice distortion, and the appearance of In-rich secondary phases such as In_2O_3.

These structural observations are in full agreement with the FESEM images, which revealed a parallel morphological evolution across the series of samples [15]. The reference film (x = 0.00) exhibited a continuous but relatively rough surface, consisting of irregularly distributed nanograins intermixed with micrometer-sized droplets and clusters (5–10 μm). These large particulates originate from laser-induced splashing and partial mercury evaporation during pulsed laser deposition (PLD), both of which disrupt the uniformity of the growing film. With the introduction of indium at low concentrations (x = 0.04–0.08), a clear improvement in surface morphology was observed. The films became smoother and more homogeneous, displaying well-distributed nanograins of approximately 25–45 nm with significantly fewer voids between neighboring grains. This enhanced uniformity suggests improved grain connectivity and a reduction in structural defects, likely due to the stabilizing influence of indium on the crystal lattice. The pronounced decrease in the number and size of surface droplets further indicates more stable plume dynamics during PLD, promoting denser film formation and the development of more effective magnetic flux-pinning centers, which are crucial for optimizing superconducting performance [16]. At the optimal doping level (x = 0.12), the film exhibited its highest structural quality, characterized by a compact, dense, and highly coherent nanograin network. The grains were tightly packed with nearly complete elimination of micro-voids, demonstrating a high degree of lattice ordering. Such morphology typically correlates with improved superconducting properties due to minimized weak-link regions and enhanced current-carrying pathways. However, at higher concentrations ($x \geq 0.16$), the trend reversed. The excessive indium substitution introduced substantial lattice strain, driving the nanograins to aggregate into larger clusters and irregular microstructures. This agglomeration degraded the overall film homogeneity and compromised the smoothness of the surface. The formation of larger grain aggregates indicates that the crystal lattice becomes increasingly unstable beyond the optimal doping limit, leading to defect accumulation and local structural distortions [17]. Consequently, the morphological deterioration at higher doping levels reflects a breakdown in film quality, consistent with the expected structural limitations of over-substituted cuprate systems.

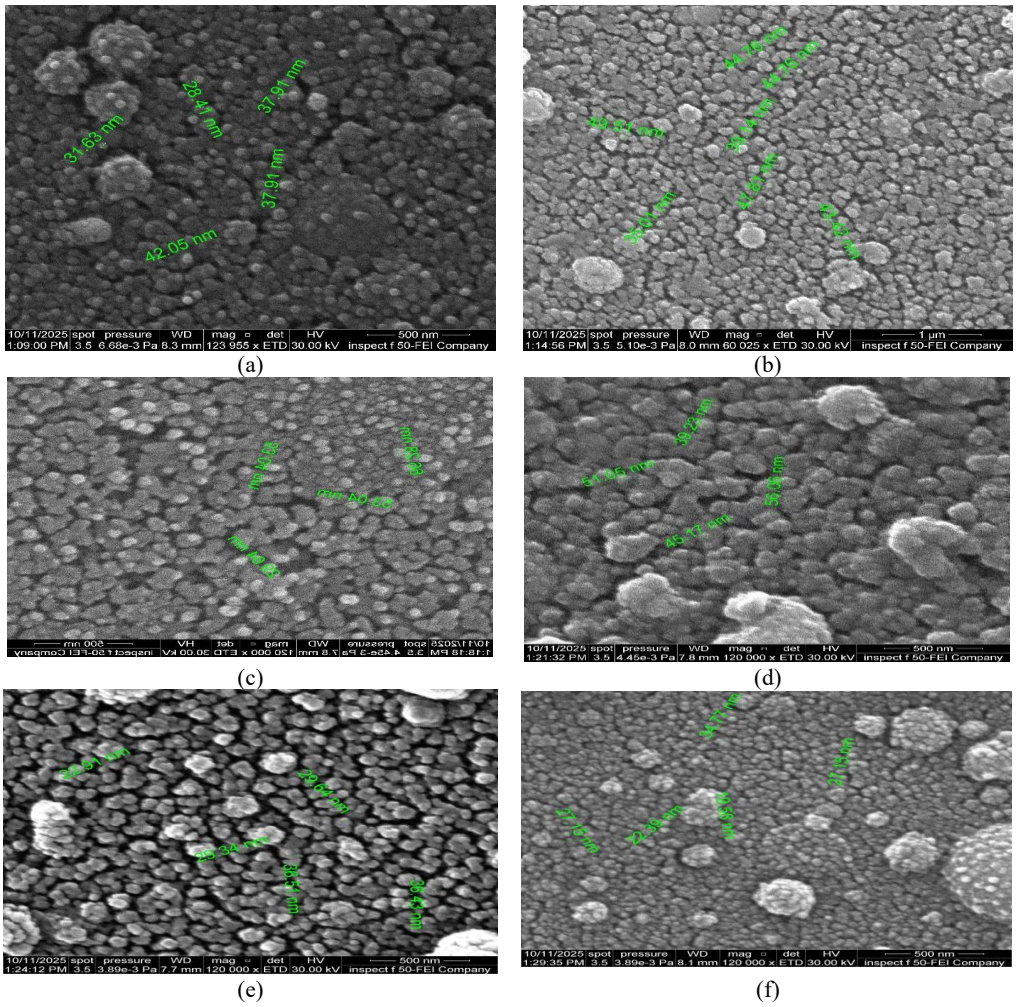

FIGURE 4. FESEM micrographs of $Hg_{1-x}In_xBa_2Ca_2Cu_{2.8}Ti_{0.2}O_{8+\delta}$ thin films at various indium concentrations: (a) x = 0.00 Irregular nanograins with micro-droplets. (b) x = 0.04 – Improved uniformity and finer grains. (c) x = 0.08 – Compact, homogeneous nanostructure. (d) x = 0.12 – Densely packed optimal morphology. (e) x = 0.16 – Grain clustering and increased roughness. (f) x = 0.20 – Irregular large particles and phase segregation.

AFM analysis further supported these findings. The quantitative surface parameters—root mean square roughness (Sq), skewness (Ssk), and kurtosis (Sku)—confirmed that the sample with x = 0.12 had the lowest roughness (Sq ≈ 4.99 nm), nearly symmetric height distribution (Ssk ≈ 0.099), and moderate kurtosis (Sku ≈ 3.81), along with the lowest surface area ratio (SA/PA ≈ 1.261). These values indicate a highly uniform, smooth, and Stable nanostructured surface [18]. For higher substitution levels (x ≥ 0.16), both the roughness and surface irregularity increased significantly (Sq ≈ 7.62 nm, SA/PA ≈ 1.517), suggesting enhanced strain and grain aggregation. Although the x = 0.20 sample showed an apparently lower roughness (Sq ≈ 2.85 nm), it's extremely high kurtosis (Sku ≈ 10.18) reflected an uneven surface likely caused by phase separation and the formation of a thin, smooth secondary In2O3 layer covering residual grains from the main phase [19].

In summary, limited indium substitution (up to x = 0.12) was found to significantly enhance the structural and morphological quality of the films. Within this range, indium effectively improved lattice ordering, reduced macrostrain, and promoted the formation of uniformly distributed nanograins with stronger intergrain coupling [20]. These improvements reflect a more stable crystal framework in which strain relaxation and controlled defect formation support coherent grain growth and improved film density. Beyond the optimal substitution level, however, excess indium introduced noticeable structural distortion and partial phase segregation. These effects manifested as surface roughening, nanograin agglomeration, and the development of micro-scale clusters, indicating a breakdown in lattice stability and an accumulation of local strain fields. Such over-substitution disrupts the ordered perovskite-like structure, leading to morphological degradation that weakens both grain connectivity and overall film quality [21]. The close agreement between XRD, FESEM, and AFM results reinforces the conclusion that x = 0.12 represents the optimal indium substitution ratio. At this composition, the film achieves the best balance between crystallographic order and morphological smoothness, exhibiting a compact nanostructure with strong c-axis orientation, minimal surface roughness, and high grain uniformity. These characteristics are essential for high-performance superconducting thin-film applications, where enhanced grain alignment and reduced defect density directly support improved electrical transport properties [22].

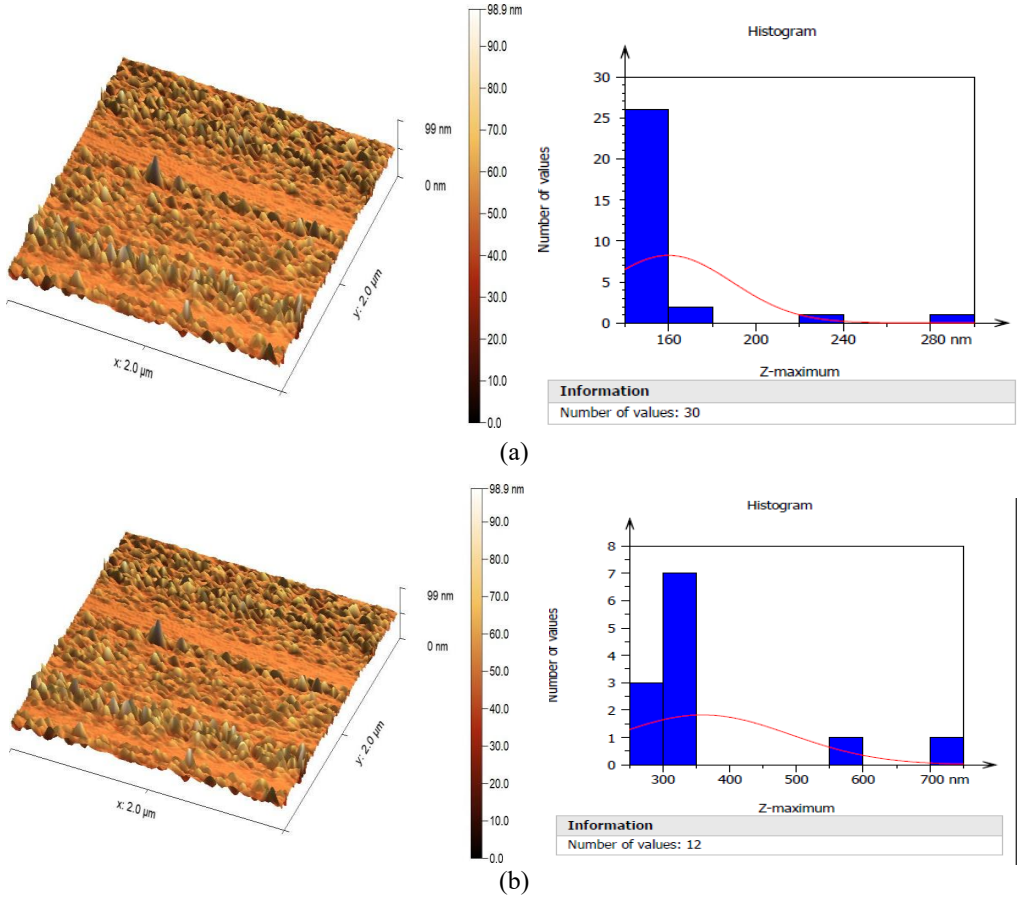

FIGURE 5. AFM 3D surface topography and corresponding height distribution histograms for $Hg_{1-x}In_xBa_2Ca_2Cu_{2.8}Ti_{0.2}O_{8+\delta}$ thin films: (a) x = 0.00 – The surface exhibits irregular nanogranular morphology with noticeable peaks and valleys, indicating moderate roughness and non-uniform grain distribution.

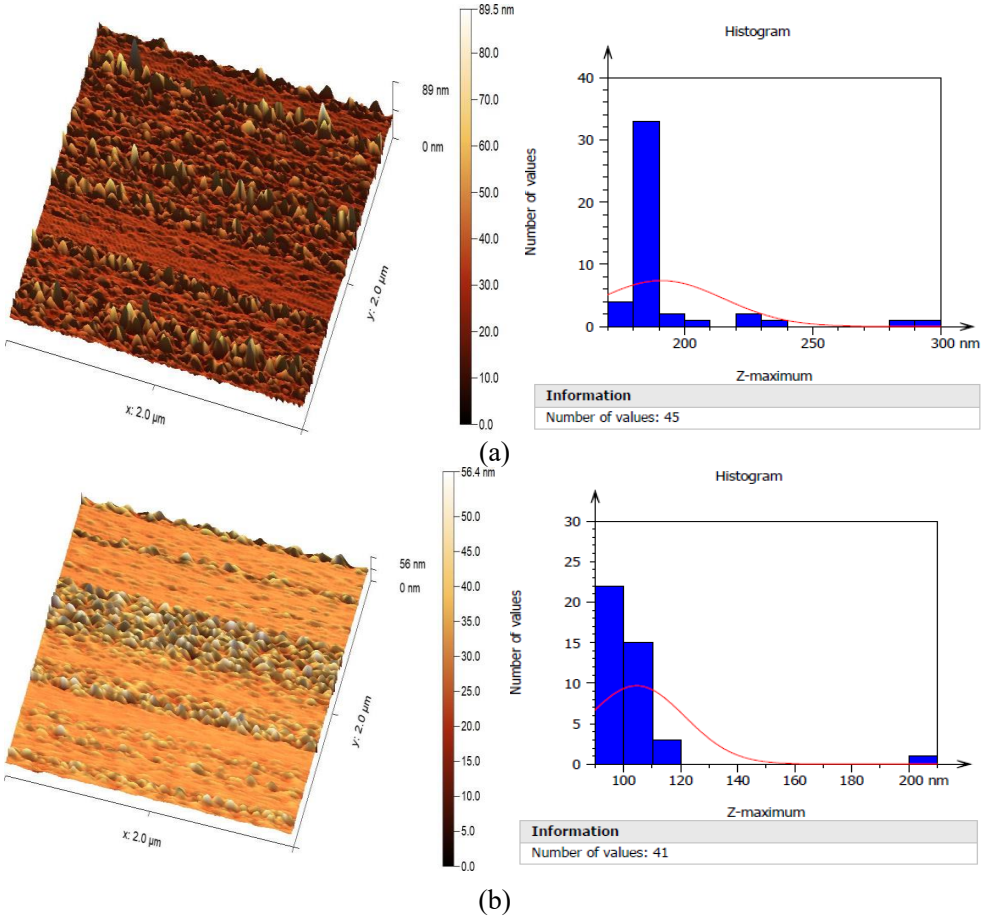

FIGURE 6. AFM 3D surface topography and height distribution histograms for $Hg_{1-x}In_xBa_2Ca_2Cu_{2.8}Ti_{0.2}O_{8+\delta}$ thin films:(a) x = 0.08 – The surface exhibits finer nanostructures with improved uniformity and reduced surface roughness, indicating more homogeneous grain growth. (b) x = 0.12 – The film shows the smoothest and most compact morphology in the series, reflecting optimal surface uniformity and stable nanocrystalline growth.

CONCLUSIONS

Thin films of $Hg_{1-In}Ba_2Ca_2Cu_{2.8}Ti_{o.20}$, were successfully fabricated using the pulsed laser deposition (PLD) technique, exhibiting uniform composition and good surface coverage. The results revealed that indium substitution had a pronounced effect on the crystallinity and surface morphology of the films. X-ray diffraction analysis showed that the optimum structural order was achieved at x = 0.12, where sharper diffraction peaks and a slight shift toward higher 20 values indicated c-axis contraction and enhanced lattice coherence.

Morphological examinations using FESEM and AFM confirmed these findings, showing dense, fine-grained, and smooth nanostructures at the same composition, while higher indium levels (x 0.16) led to grain clustering, surface roughness, and partial phase segregation. Overall, the study concludes that a moderate level of indium substitution (x = 0.12) yields the most stable and compact nanostructure, representing an effective approach for improving the microstructural quality of Hg-based cuprate superconducting thin films and potentially enhancing their functional performance.

REFERENCES

1. Maeda, H., et al., A new high-Tc oxide superconductor without a rare earth element. Japanese Journal of Applied Physics, 1988. 27(2A): p. L209.
2. Xu, Q., et al., Microstructure and Superconductivity in Bi–Sr–Ca–Cu–O System Doped with Pb and Sb. Japanese journal of applied physics, 1990. 29(10R): p. 1918.
3. De Biasi, R. and S. Araujo, Influence of the annealing parameters on the volume fraction of the high-Tc phase in the Bi-Sr-Ca-Cu-O system. Journal of Magnetism and Magnetic Materials, 1992. 104: p. 471-472.
4. Wadia, K.M., Abdulateefa, A.N., Shabanb, A.H., Jasimb, K.A., Improvement of superconducting properties of Bi 2 Ba 2 Ca 2 Cu 3 O 10+δ Ceramic by prepared under different pressures, Energy Procedia, 2019, 157, pp. 222–227.
5. Dawud, A., The effect of n variation on the high-Tc super. behavior of the Bi2Sr2Can-1CunO2n+ 4 system. 2000, Ph. D. Thesis, Al-Nahrin University, College of Science.
6. Hermiz, G., Thermal Analysis &Phase Transformation HTSc of (Bi1-xPbx) 2 (Sr1-yBay) 2Ca2Cu3O10+ δ compound. 2001, Ph. D, Baghdad University.
7. Haider, H.M.J., Wadi, K.M., Mahdi, H.A., Jasim, K.A., Shaban, A.H., Studying the partial substitution of barium with cadmium oxide and its effect on the electrical and structural properties of HgBa2Ca2Cu3O8+δ superconducting compound, AIP Conference Proceedings, 2019, 2123, 020033.
8. Shaban, A.H., Mohammed, L.A., Hussein, H.S., Jasim, K.A., The structural properties of Y1-XLaXBa4 Cu7 O15+ δ superconductor compound, Digest Journal of Nanomaterials and Biostructures, 2022, 17(2), pp. 519–525.
9. Omar, B.A., Fathi, S.J., Jassim, K.A., Effect of Zn on the structural and electrical properties of high temperature HgBa2Ca2Cu3O8+δ superconductor, AIP Conference Proceedings, 2018, 1968, 030047.
10. Mohammed, L.A., Jasim, K.A., Improvement the superconducting properties of TlBa 2 Ca 2 Cu 3x Nix O 9-δ superconducting compound by partial substitution of copper with nickel oxide on the, Energy Procedia, 2019, 157, pp. 135–142.
11. Jasim, K.A., Makki, S.A., Almohsin, A.A. Comparison study of transition temperature between the superconducting compounds Tl0.9 Pb 0.1Ba2Ca2Cu3O9, Tl0.9Sb0.1Ba2Ca2Cu3O9-δ and Tl0.9Cr0.1Ba2Ca2Cu3O9-δ, Physics Procedia, 2014, 55, pp. 336–341.
12. Abdulateef, A.N., Alsudani, A., Chillab, R.K., Jasim, K.A., Shaban, A.H., Calculating the mechanisms of electrical conductivity and energy density of states for Se85Te10Sn5-xInx glasses materials, Journal of Green Engineering, 2020, 10(9), pp. 5487–5503.
13. Jasim, K.A., Alwan, T.J., Effect of Oxygen Treatment on the Structural and Electrical Properties of Tl0.85Cd0.15Sr2CuO5−δ,Tl0.85Cd0.15Sr2Ca2Cu2 O 7−δ and Tl0.85Cd0.15Sr3Ca2Cu3 O 9−δ Superconductors, Journal of Superconductivity and Novel Magnetism, 2017, 30(12), pp. 3451–3457.
14. Jasim, K.A., The effect of cadmium substitution on the superconducting properties of Tl1-xCdxBa2Ca2Cu 3O9-δ compound, Journal of Superconductivity and Novel Magnetism, 2013, 26(3), pp. 549–552.
15. Al-Khafaji, R.S.A., Jasim, K.A., Dependence the microstructure specifications of earth metal lanthanum La substituted Bi2Ba2CaCu2–XLaXO8+δ on cation vacancies, AIMS Materials Science, 2021, 8(4), pp. 550–559.
16. Aleabi, S.H., Watan, A.W., Salman, E.M.-T., kareem Jasim A.,Shaban, A.H., Alsaadi, T.M., The study effect of weight fraction on thermal and electrical conductivity for unsaturated polyester composite alone and hybrid, AIP Conference Proceedings, 2018, 1968, 020019.'
17. Ahmed, B.A., Mohammed, J.S., Fadhil, R.N., ...Shaban, A.H., Al Dulaimi, A.H., The dependence of the energy density states on the substitution of chemical elements in the Se6 Te4-xSbx thin film, Chalcogenide Letters, 2022, 19(4), pp. 301–308.
18. Kadhim, B.B., Khaleel, I.H., Hussein, B.H., ...Al-Maiyaly, B.K.H., Mahdi, S.H., Effect of gamma irradiation on the TlBa2Ca2Cu3O9-δ superconducting properties, AIP Conference Proceedings, 2018, 1968, 030054.
19. Jassim, K.A., Thejeel, M.A.-N., Salman, E.M.-T., Mahdi, S.H., Study characteristics of (epoxy-bentonite doped) composite materials, Energy Procedia, 2017, 119, pp. 670–679.
20. Watan, A.W., Aleabi, S.H., Risan, R.H., Jasim, K.A., Shaban, A.H., Preparation and Physical Properties of Doped CdBa2-x SrxCa2Cu3O8+δ Compound, Energy Procedia, 2017, 119, pp. 466–472.
21. Nkum, R., M. Gyekye, and F. Boakye, Normal-state dielectric and transport properties of In-doped Bi–Pb–Sr–Ca–Cu–O. Solid state communications, 2002. 122(10): p. 569-573.
22. Liang, B., et al., Phase evolution, structural and superconducting properties of Pb-free Bi2Sr2Ca2Cu3O10+ δ single crystals. Superconductor Science and Technology, 2004. 17(6): p. 731.